Archives of Civil and Mechanical Engineering (2024) 24:146
https://doi.org/10.1007/s43452-024-00960-3

ORIGINAL ARTICLE

The influence of laser texturing on the tribological behavior of titanium alloy Ti6Al4V in medical applications

Anna Woźniak[1] · Oktawian Bialas[1] · Marcin Adamiak[1] · Branislav Hadzima[2] · Janusz Szewczenko[3]

Received: 12 November 2023 / Revised: 3 April 2024 / Accepted: 24 April 2024

Abstract

This paper analyzes the tribological behavior of the Ti6Al4V ELI alloy subjected to laser texturization for medical purposes. Laser texturing enables one to observe specific patterns of the material surface at established depths. Microtexturing of the samples was performed using a 355 nm picosecond laser. The influence of the microtexturing process (depending on the process parameters) on the geometric parameters of the proposed laser texturing pattern was evaluated. Selected samples were subjected to tribological testing using the ball-on-plate technique in dry and lubricant-sliding methods (in Ringer solution). The wear properties were evaluated by comparing the coefficient friction, wear volumes, and wear ratio. A scanning electron microscope characterized the morphologies of the wear scar and the wear mechanism. The experimental results show that the surface texturing and the changes in microgrooves can reduce wear. The results indicate, that samples after laser texturing were characterized by 15% higher microhardness, compared to those in the initial state. It was found, a 26% reduction in friction coefficient and 29% in the wear volume compared to the smooth, untextured surface samples under lubricated conditions. The decrease in value of the coefficient friction and wear volume for the samples after the laser texturing process is an effect of synergistic of entrapped wear debris in micro-grooves and increased hardness for samples after laser textured.

Keywords Ti6Al4V · Laser texturing · Tribology test · Microscopic observation

1 Introduction

Currently, there is a noticeable increase in endoprosthesis implantation procedures worldwide. Furthermore, there is a recognized need to enhance the functional properties of biomaterials to ensure harmonious interaction within the implant–human body tissue system. As indicated by Pereira et al. [1] failures of endoprosthesis reconstructions range from 40 to 73% at 5 to 15 years. Titanium and its alloys are one of the most popular materials in the biomedical applications, because of their excellent corrosion resistance, ability to spontaneous oxide layer formation, and satisfying mechanical properties [2]. However, the main disadvantage of titanium materials is their poor tribological properties (including fretting wear), witch during the implantation have a significant effect on the implant's life. Iwabuchi et al. [3] compared the friction and fretting wear resistance of three common biomaterials: Co39Cr6Mo alloy, Ti6Al4V alloy, and SU304 steel. Ti6Al4V alloy exhibited good resistance to fretting wear it also showed the highest wear compared to other materials based on friction wear test. Similarly, Beake et al. [4] reported that the wear resistance of the Ti6Al4V alloy was lower than that of most metallic biomaterials. Decreased wear resistance can reduce the effectiveness of the implants and may contribute to massive tissue loss in the surrounding area. Additionally, intensive material degradation can lead to the release of elements/corrosion products, causing local toxic reactions in the surrounding tissues, and next eventual metallosis (in effect of accumulation degradation products, issuing tissue harm) [5]. Furthermore, in tribological contact, wear residues can oxidize and aggregate, increasing the degree of wear (wear increased by

✉ Anna Woźniak
anna.wozniak@polsl.pl

[1] Materials Research Laboratory, Faculty of Mechanical Engineering, Silesian University of Technology, Konarskiego 18A Street, 44-100 Gliwice, Poland

[2] University of Zilina, Univerzitna 8215/1, 010 26 Zilina, Slovakia

[3] Department of Biomaterials and Medical Devices Engineering, Faculty of Biomedical Engineering, Silesian University of Technology, Roosevelta 40 Street, 41-800 Zabrze, Poland

Published online: 09 May 2024

corrosion). Therefore, modifying the surface properties of titanium implants is still recognized as an essential method to improve biocompatibility.

Conradi et al. [6] pointed that the surface laser texturing has been recognized as an effective method to enhance the tribological performance of materials. Laser texturing is a precise, accurate, reproducible, and environmentally friendly surface modification method. These advantages made laser-texturing an unbeatable process to other texturing methods, such as embossing, vibro-rolling, abrasive jet machining, micro-coining, roller-coining, micro-casting, reactive ion beam etching, electrical discharge machining, as showed by Reddy et al. [7]. Many research showed [8–11], that laser-texturing of metal base materials can lead to a change in the interaction between surfaces in friction contact, resulting in better lubrication and enhanced wear resistance. However, the size, depth, and density of the laser-textured pattern have significant effects on the degree of wear and the coefficient of friction. Lin et al. [12] highlighted the main advantages of laser-textured surfaces as the potential for continuous lubrication owing to the presence of lubricant on the textured surface and the entrapment of wear debris, thus reducing overall wear. In literature data, to improve the tribological behaviour of biomaterials, researchers have proposed texture patterns such as micro-dimple array [13, 14], micro-groove cross-hatched [9, 15–17], and groove system forming trust [18]. Wang et al. [10] demonstrated the coefficient friction of the laser-textured surface with periodic surface structures was reduced by approximately 70–80% compared to the original Ti6Al4V alloy surface. Similar results were observed by Song et al. [9]. Interestingly, Sadeghi [13] owed that the density ratio of grooves significantly affects wear behavior. The obtained results indicated that increasing the density of the dimples (laser texture pattern) from 6.5 to 21% resulted in wear reduction. Furthermore, Wang et al. [19] demonstrated that laser microtexturing can alter surface chemistry, such as the wetting angle, through structural morphology changes, thereby offering a broad spectrum of practical applications.

Despite extensive investigations on the surface texturing of titanium and its alloys using laser techniques, limited studies have been focused on the texturing using Nd: YAG, CO_2, or nanosecond laser. In our work, we decided to use the picosecond laser system. It must be taken into account that lasers with short or ultrashort pulse duration (in the picosecond or femtosecond range) provide a higher quality surface compared to systems equipped with nanosecond or longer laser pulses, which suggested Grabowski et al. [20]. Furthermore, picosecond laser ablation creates a heat-affected zone (HAZ) less than < 1 mm wide-for comparison. Compared to the conventional long-pulse laser, ultrashort pulse systems have high peak energy in short time. In effect, picosecond laser surface texturing can keep a high precision and reduce the thermal effect. Additionally, studies presented in the literature data often focused on used laser systems with high laser power [6, 21–23]. Even in the research based on using ultra-short pulse duration, the power of the laser system was high [15]. Using a lower energy power could be particularly relevant for medical applications where minimizing heat-affected zones and maintaining the integrity of the material are critical. Heat generation can induce residual stresses in the material, which may contribute to issues like cracking, distortion, or fatigue failure over time. In the case of implants, minimizing residual stresses is essential to prevent premature failure and ensure the long-term stability of the implant within the body. Medical implants often require a high degree of precision, especially when tailored to fit specific patient anatomies. Excessive heat can lead to imprecise machining and may hinder the customization of implants. Minimizing heat-affected zones allows for more precise control over the manufacturing process, facilitating the creation of implants with accurate dimensions and shapes.

The main objective of our investigation was to improve the wear properties of the Ti6Al4V alloy for biomedical applications. Our challenge was to modify the alloy surface using a laser texturing process to achieve the optimal tribological response in both lubricated and dry conditions. A picosecond laser was used to prepare 12 textured patterns, dependent on texturing process parameters. As a laser pattern, we proposed a groove system forming a truss, because of the obtainable better tribological behaviour, that was reported in literature data and that was cited in our paper. This article will be focused on morphology changes after the laser texturing process and tribological behaviour. Tribological testing was performed on the samples using the pin-on-plate technique in both dry and lubricant-sliding (in Ringer solution) forms to gain comprehensive insight regarding the use of Ti6Al4V in biomedical applications. Additionally, the surface morphology, microstructure, and hardness tests of the surface were examined.

2 Materials and methods

Experiments were performed on Ti6Al4V ELI titanium alloy samples with a chemical composition that met the requirements of ISO 5832-3 standard [24] and are given in Table 1. The cub samples with edge length of 10 mm were obtained using the selective laser melting (SLM) method according to the procedure described in our previous article [25]. The dimensional accuracy of the samples was ± 0.2 mm.

First, samples were subjected to mechanical treatment, which included grinding and polishing using the Tergamin-30 machine (Struers, Ballerup, Denmark). Samples

Table 1 Chemical composition of the Ti6Al4V titanium alloy

Element, wt. (%)	Al	V	Fe	O	C	Ni	H	Ti
Declared	5.50–6.50	3.50–4.50	≤0.25	≤1.13	≤0.08	≤0.05	≤0.012	Rest
ISO 5832-2	5.50–6.75	3.50–4.50	≤0.3	≤0.2	≤0.08	≤0.05	≤0.015	Rest
Measured	5.90	3.95	<0.1	–	–	–	–	Rest

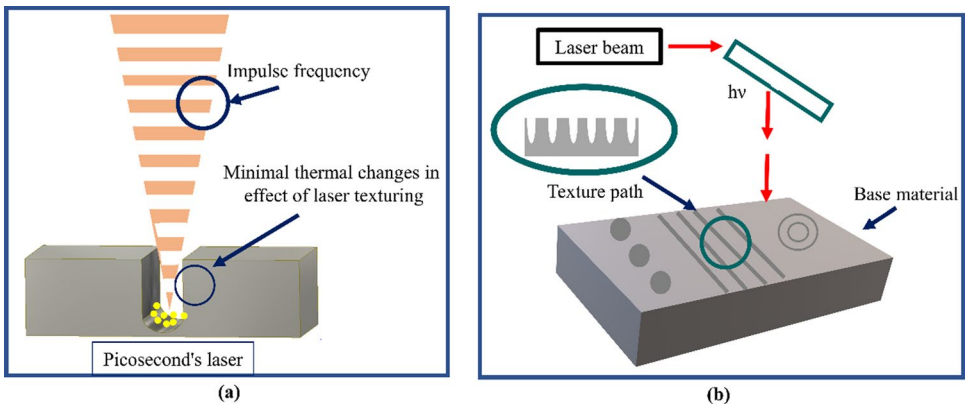

Fig. 1 Schematic diagrams of: **a** a laser micromachining system and **b** the impact of the laser beam on the solid matter

were wet-grounded down to P800, P1200, P2400, and P4000 grid/mm^2 using silicon carbide (SIC) papers. For polishing, a colloidal silica suspension of OP-U 0.04 µm was used. Finally, all samples were cleaned sequentially in acetone and then deionized water with ethanol (2:1) using an InterSonic IS-1 ultrasonic cleaner (InterSonic S.C., Olsztyn, Poland), and finally dried. After mechanical treatment, the tests were conducted on the samples under the name **P_is** (initial state). The average surface roughness after grinding and polishing was measured to be about $R_a = 0.39$ µm, and $R_q = 0.54$ µm.

The surface texturing process was performed using an A-355 picosecond laser system (Oxford Lasers Ltd, Didcot, UK), equipped with a 335 nm wavelength, diode-pumped solid-state picosecond laser which generates 5–10 ps pulse durations of 120 µJ at 400 Hz pulse frequency. The average laser power for the texturing system was 24 mW. The laser beam intensity distribution is Gaussian. A picosecond laser beam emission guarantees the ablation process, wherein high-energy laser radiation quantum results in a decrease in the bond strength between the atoms (Fig. 1a). As a result, the atoms evaporate layer by layer. Interaction between the focused laser beam and the surface of the material results in the absorption of the photon energy by the activated atoms and their next evaporation (ablation). The quality of the laser texture process depends on the laser source, i.e. laser intensity, pulse duration, laser wavelength, as well as material properties of the material being laser textured. Picosecond laser systems emit pulses of linearly polarized light with the Gaussian intensity distribution. Picosecond lasers have a greatly reduced heat load and heat-affected zone in the textured material compared to nano- and micro-second lasers (Fig. 1b). Additionally, the short pulse length leads to

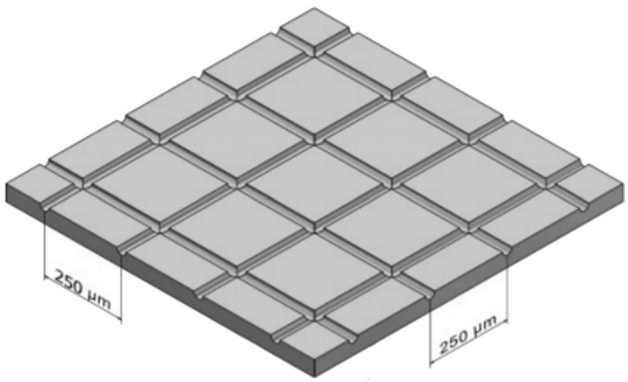

Fig. 2 Schematic diagram of laser texturing pattern

higher energy intensities, and early evaporation of materials can be achieved through rapid heating. All samples were textured under the same conditions, at room temperature ($T = 22.5 \pm 1$ °C, humidity 53 ± 1%), and assisted with a jet of air to remove debris produced during processing.

The laser pattern (or filling strategy) was designed with the Cimita software (Oxford Lasers, Didcot, UK) integrated into the micromachining system. The path of the laser texturing was a groove system forming a truss with a groove space of 250 µm. The proposed laser texture demonstrates a groove density factor of 17%. The laser beam was focused on the sample surface to achieve a diameter of 30 µm (Fig. 2). A total of eight laser texturing parameter conditions were defined. The fixed laser process parameters are summarized in Table 2. Five samples of each condition were produced. However, the truss laser pattern also was selected because of the possibility of obtaining better microbiological properties

Table 2 Laser texturing process parameters

No	Name	N, number of the passes of the laser beam	Laser scan speed (mm/s)	Frequency (Hz)	Laser power (mW)	Beam width (μm)	Beam quality factor M^2
1	P1	6	1	400	48	30	< 1.2
2	P2		0.5				
3	P3	8	1				
4	P4		0.5				
5	P5	10	1				
6	P6		0.5				
7	P7	12	1				
8	P8		0.5				

due to the contact guide effect, which we want to be tested and published in the next manuscript, which will concentrate on physicochemical, electrochemical, and biological properties of laser textured titanium biomaterials. Interestingly, in the literature data, it can be found that the influence of the laser texturing of metal biomaterials surface on cell activity and proliferation. Mahmud et al. [26] showed directional migration of cancer cells was demonstrated for the system of microgrooves on the biomaterial's surface. The results of the analyzes were consistent with the contact guidance effect (a phenomenon correlating the shape of the substrate surface with the direction of cell proliferation), indicating the possibility of changing cell expression as a result of the formation of a specific texture pattern, which was described by Raimbault et al. [27]. The phenomenon may also contribute to limiting the adhesion of bacteria to textured surfaces. Studies conducted by Chebolu et al. [28] indicate the antibacterial properties of textured surfaces. Veiko et al. [29] conducted a comparable in vivo study using dental implants with different laser patterns: continuous micro-grooves with a width and depth of about 20–50 μm, discrete micro-cavities, and irregular laser topography. Based on histological analysis, it was found that samples with micro-grooves laser pattern exhibited the highest BIC parameter (bone-to-implant contact) and contained the highest number of mature osteocytes, indicating the best secondary stability and osseointegration.

The surface topography and the microstructure of the samples were evaluated using a Supra 35 high-resolution scanning electron microscope (SEM) (Zeiss, Oberkochen, Germany) with 50–500 kx magnification. In addition, the microstructure and surfaces of the tested samples were investigated using electron backscatter diffraction (EBSD) and secondary electron (SE) modes, respectively, during SEM analysis. The geometrical parameters of the laser-textured samples were determined using ImageJ software. Firstly, the SEM image was converted to a 32-bit grayscale. Subsequently, the image was transformed into a binary (black and white) representation, applying thresholding. After setting the scale, the measurements were carried out automatically according to the ImageJ algorithm.

The tribological properties of the tested samples were investigated using the ball-on-plate method using a CSM tribometer (CSM Instruments, Needham, MA USA). Sliding in ball-on-plate mode was selected to more closely simulate the conditions typical of biomedical applications, despite this mode being difficult to provide uniform and constant contact conditions, as suggested by Conradi et al. [6]. As a counter sample, an Al_2O_3 ceramic ball with a 6 mm diameter was used. A relatively small ball diameter was selected to simulate the critical contact condition with very small contact areas and high contact pressure. The maximum contact pressure was calculated using Hertzian contact theory for spherical counter-samples and planar-tested samples, according to Eq. (1).

$$P_{\max} = \frac{3F}{2\pi a^2} \tag{1}$$

where P_{max}—maximum contact pressure (GPa), F—normal (applied) load (N), a—contact radius (mm)—which is calculated according to Eq. (2).

$$a = \sqrt[3]{\frac{\frac{3F}{8} \cdot \left(\frac{1-\nu_2^2}{E_1}\right) + \left(\frac{1-\nu_2^2}{E_2}\right)}{\frac{1}{d_1} + \frac{1}{d_2}}} \tag{2}$$

where $\vartheta_{1/2}$—Poisson's ratio, $E_{1/2}$—Young's modulus (GPa), $d_{1/2}$—diameter of curvature (mm), 1—tested samples (Ti6Al4V alloy), 2—counter samples ball Al_2O_3.

To determine the Hertzian pressure, mean values of the Poisson's ratio (0.23 and 0.32 for Al_2O_3 and Ti6Al4V titanium alloy, respectively) and Young's modulus (380 and 103 GPa for Al_2O_3 and Ti6Al4V titanium alloy, respectively) were assumed. The radius of the ceramic ball was 3 mm, and the surface of the tested samples was unlimited (flat surface). Normal loads of 3, 6, and 9 N were

used, which correspond to Hertzian pressures of 800, 950, and 1160 MPa, respectively. According to literature, a 1000 MPa Hertzian pressure is considered critical in many biomedical applications [6]. The stroke length was fixed at 6 mm and the frequency was 1 Hz creating a sliding speed of 1.2 cm/s. Fisher [30] pointed that, the sliding velocity (under the velocity of normal walking conditions) of the knee or hip implants varies a lot among different people ranging from 0 to 60 mm/s. However, it must be taken into account that the sliding velocity has a significant effect on the lubrication regime. Increasing sliding velocity leads to the formation of thicker lubricant film. In effect, under the hydrodynamic situation, the tribological performance of artificial joints will be better than the inner boundary lubrication [31].

Dry and lubricated (fully flooded) tests in Ringer solution (8.6 g/cm^3 NaCl, 0.3 g/cm^3 KCl, 0.33 g/cm^3 $CaCl_2 \cdot 2H_2O$), were carried out in room conditions at a relative humidity (RH) of 50% at ambient temperature. Also, Conradi el al. [6] and Wang et al. [32] performed tribological test in simulated body fluid solution. The coefficient of friction (μ) during sliding was continuously recorded. Five samples from each group were subjected to wear behavior analysis, and for each sample, the tests were conducted five times to ensure the validity of the data.

The Surtronic 35 profilometer (Taylor Hobson, UK) was used to measure of the cross-sectional area of the wear tracks (wear volume, V_w). For each wear track, five wear volume measurements were taken. Next, the specific wear rate, K_r was calculated using Eq. (3), as proposed Ju et al. [33]

$$K_r = \frac{V_w}{F_n \times t} \tag{3}$$

where K_r—wear ratio (mm^3/N min), V_w—wear volume (mm^3), F_n—normal load (N), t—total time (min).

The hardness of the samples subjected to the wear test was evaluated, using a microhardness tester (Future-Tech FM-ARS), applying a load of 100 gf for 15 s. For each sample, five measurements were performed.

The digital microscope DVM6 (Leica, USA) was used to show the location of microhardness testing (Fig. 3) and the sample's cross-section with entrapped wear debris after the wear test.

All data were expressed as mean ± SD.

3 Results

The surface morphology of the samples after the laser texturing process is shown in Fig. 4. For all of the tested sample groups, cross-like micro-groove patterns were observed which are characteristic features of photothermal ablation (Fig. 4a). In this sense, transverse and parallel cuts demonstrated the wavy profile which constitutes the texture. The lined grooves array was regular and uniform. The average width between the laser paths was 246 ± 4 µm which corresponded to the designed laser texture pattern (Fig. 2). From the cross-sectional view, the presence of sidewalls in the resolidified material along the laser paths was observed. Huerta-Murillo et al. [34] referred to these features as microbulges or micro-crowns (Fig. 4b).

Laser exposition causes the material to melt and evaporate, creating grooves. When temperature and vapor pressure increased in the groove, the molten material was ejected and began to accumulate along the sides of the micro-groove, which created a micro-bugle. The surface of the micro-bugle exhibited the presence of spontaneously arranged, partially melted sub-or nanoparticles and cracks. Additionally, a large number of spherical particles along the laser paths were observed (Fig. 4c), whereas the flat areas between laser-scanned paths were covered with fewer small, circular particles, and debris (Fig. 4c). A similar observation was presented by Wang et al. [35]. However, the morphology of the top and bottom surfaces along the laser path was different (Fig. 4d and e), due to the position of the samples in the working chamber, especially relative to the flow-air system (used to remove nonmelted material debris) during the texturing process (Fig. 5). Spherical voids were visible along the top side of the laser paths, which were perpendicular to the airflow direction, that made up the inner surface of the square texture pattern (Fig. 4d). Along the bottom surface of that same path, a greater number of spherical particles

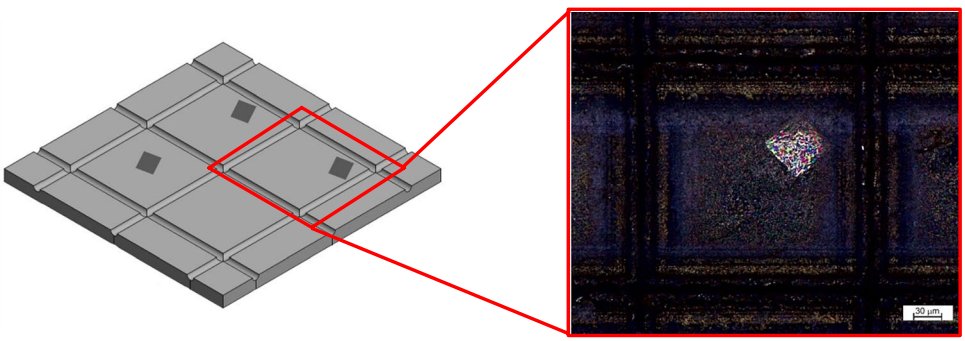

Fig. 3 Examples location of microhardness measurements of P3 samples group

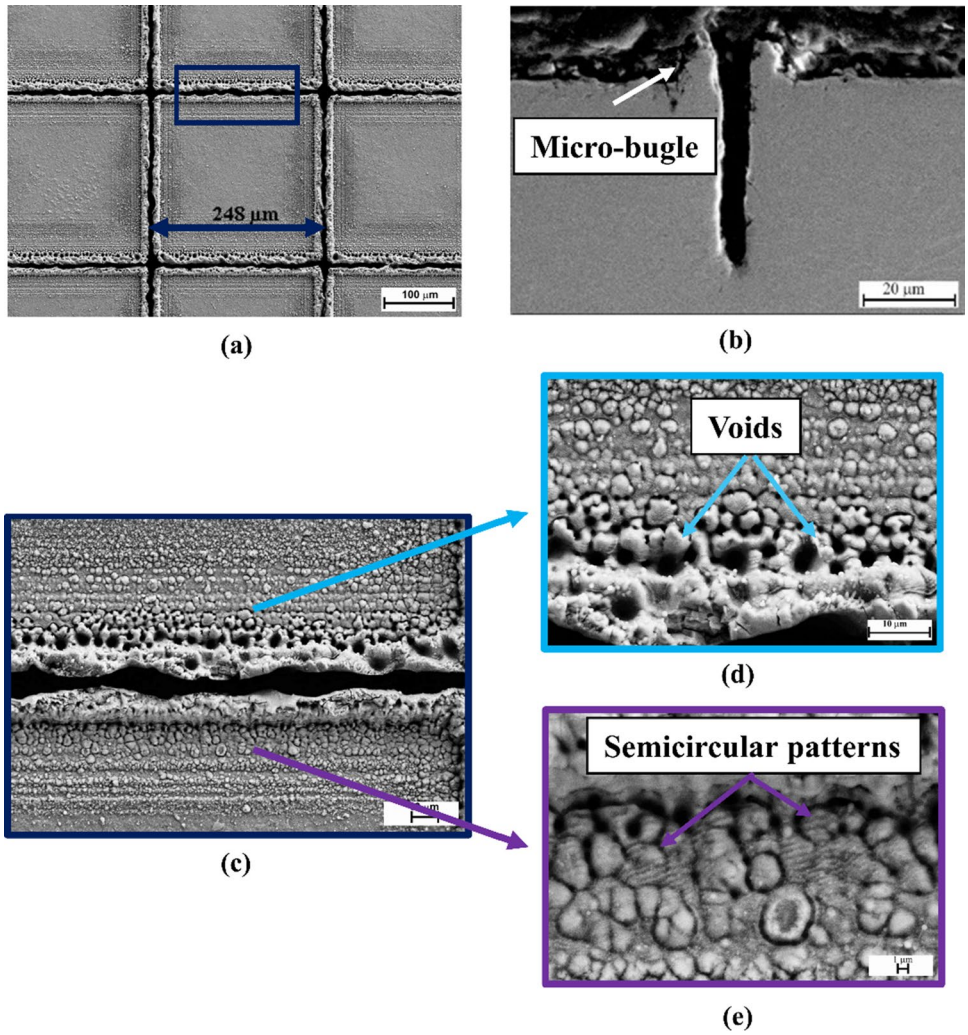

Fig. 4 Examples of sample surface morphology after laser texturing: **a** texture pattern, **b** transverse cut of single laser track, **c** top view of single laser track, **d** voids along the laser track, and **e** spherical particles along laser track

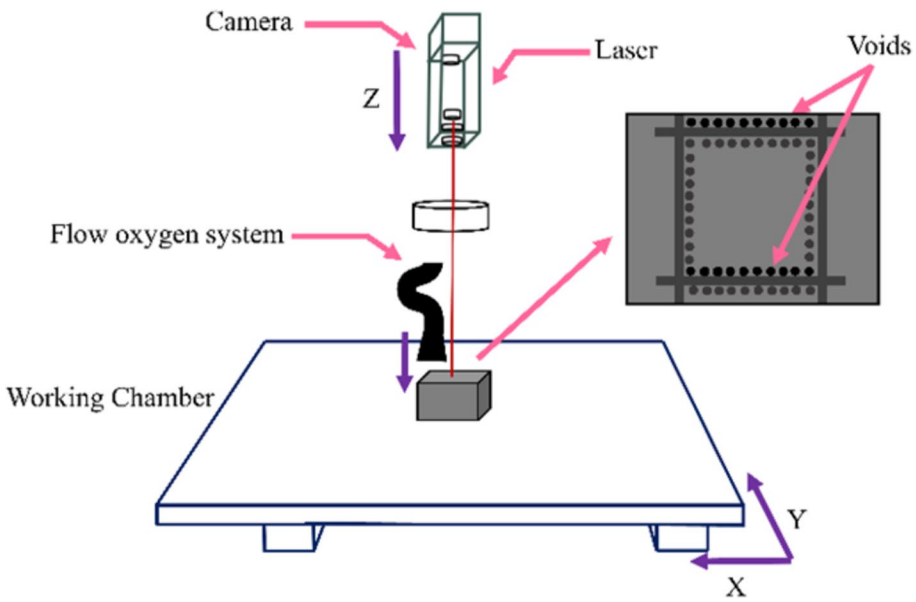

Fig. 5 Scheme of the laser texturing system

were visible, which were created by metal vapor re-solidification, according to the micro-bugle formed process. In addition, some particles consisting of multiple semicircular patterns were observed, which formed due to the overlapping of subsequent laser pulses. One can assume that some particles found on the top side of the path were poorly bonded with the substrate material surface. As a result of the air blowing through, these particles broke out, creating voids. Additionally, the heat-affected zone was negligible (thickness was less than 1 μm) for all of the tested samples based on SEM observation. Laser texturing is considered a thermal-controlled process, wherein the laser is the source of heat. Localized heat build-up induces a heat-affected zone around the textured area, which might promote oxidation and microstructural changes near the surface. However, the heat transfer into the substrate material might be limited if a laser beam system with short time impulse (i.e., pico-or nanoseconds long) is used.

SEM micrographs revealing the surface topography and cross sections of samples textured using various parameters and groove profiles are shown in Fig. 6. For the samples textured using a 0.5 mm/s laser beam speed (i.e., samples P1, P3, P5, and P7), the grooves paths were regular and rectilinear regardless of the number of laser beam passes. Moreover, minimal residual non-vaporized material in the grooves was observed in the cross-sectional views. However, for the samples textured using a 1 mm/s laser scan speed (i.e., samples P2, P4, P6, and P8), harmonic waveforms of the grove path were observed. Additionally, the amount of surface-bound, non-evaporated material residues in the groves increased too.

The characteristic parameters describing the texture shape of all tested samples group were presented in Fig. 7. It was found, that with decreasing value of laser speed from 1 to 0.5 mm/s, for that same number of laser passes, the depth of the grooves increases. Additionally, at first with increasing the laser passes number, the depth of the groves increases. The lowest grove's depth was recorded for the samples textured using passes number of laser $N=6$. Increasing the number of passes to $N=8$, caused an increasing value of the grove's depth to 35.2 ± 3.1 μm for $V=0.5$ mm/s, which was the highest value measured in the tested group. However, further, an increase in the number of passes to 10, and next to 12, no significant change in the depth of the grooves caused. It was reported that with increasing depth of grooves, the height of the micro-bugle increased too. Additionally, the width of the texture groove for all tested samples was in the range of 9.9–12.5 μm.

Therefore, one can conclude that the surface topography and morphology changes of the tested samples depended on

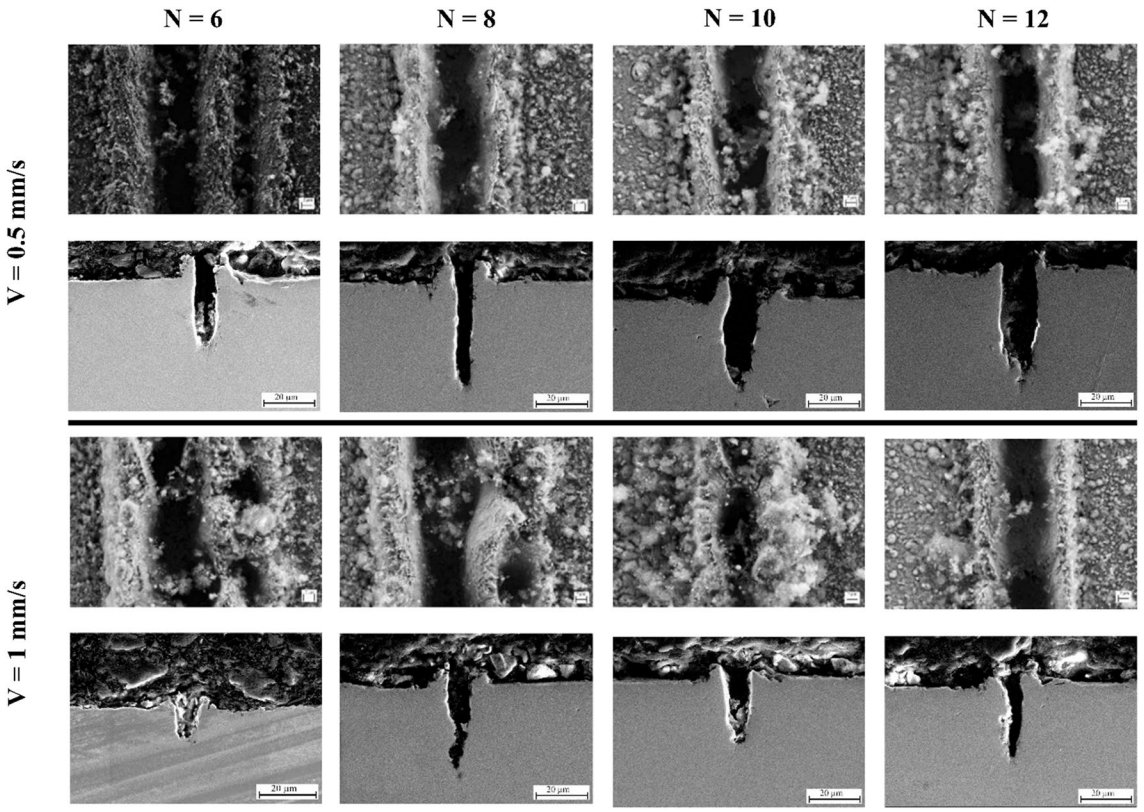

Fig. 6 SEM micrographs revealing sample texturing as a result of the speed of the laser beam (V) and number of laser beam passes (N)

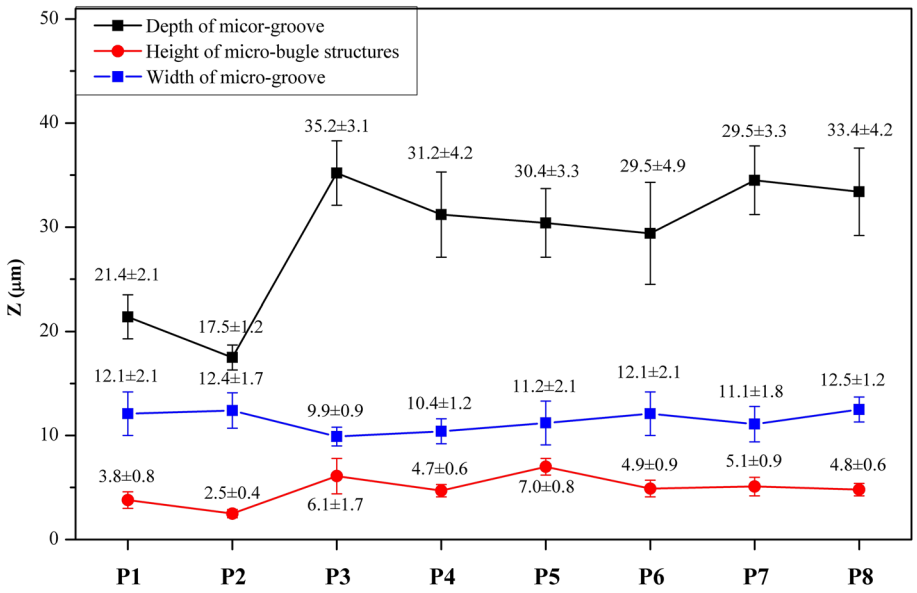

Fig. 7 Geometric dimensional changes of samples after laser texturing, where *Z* is the depth or weight of the micro-groove or height of micro-bulge structures

the energy deposited and absorbed on the textured surface as well as the velocity of the vapor and solidification process during the thermal cycle [36]. Using a slower scan speed during the texturing process results in both an increase in deposited energy in the material and increased surface temperature. Consequently, the amount of melted material increases giving rise to greater groove depths and micro-bugles. The results are comparable to those reported by Huerta-Murillo et al. [34]. During subsequent laser passes, the material surface is reprocessed, which leads to increasing groove depths. These results corresponded with a logarithmic dependence between laser pulse energy and square diameter for the clean ablation mechanism in metals during laser pulse integration, reported by Mannion et al. [37]. However, no significant changes were observed in the geometric dimensions of the groove's structures after 8 or more laser beam passes (samples P 5–8). Laser focal length disturbances after obtaining the maximum groove depth (sample P3) may cause a lack of changes in the groove's structural features. Additionally, the plasma shielding effect may also contribute to this effect, which was most apparent for samples textured using a 0.5 mm/s laser speed for 10 or 12 laser passes. With decreased laser speeds, the interaction time between the laser beam and the irradiated surface increases. Giorleo et al. [38] and Hauert [39] suggest that this leads to the formation of a plasma plume, which causes laser energy absorption and is a barrier to metal evaporation. Therefore, the evaporation of the material favors the rapid solidification of the plasma. The width of the grooves ranged from 10–12 µm, which is less than that of the designed laser process pattern (laser beam diameter 30 µm), regardless of the textured parameters. This is because injected material settles on the previously formed micro-bulges, which will increase the width of the lined hump structure on the surface. Similar results were reported by Tang et al. [40] after subjecting aluminum-based alloys to laser texturing.

The laser beam is absorbed by free electrons in the thin layer (optical absorption depth δ_α), which is inversely proportional to the value of the absorption coefficient of the material. A laser texturing system equipped with a 355 nm wavelength and 15 nm optical absorption depth for Ti6Al4V titanium alloy was used in these experiments, as was calculated by Palik [41]. During the texturing process, it is necessary to know when the metal's surface begins melting, ablating (vaporizing), and boiling. Grabowski et al. [42] determined the threshold of fluency when the surface of the Ti6Al4V alloy starts to melt and vaporize for different pulse durations according to Fig. 8, wherein diagonal lines represent the constant temperature of melting and boiling points as indicated.

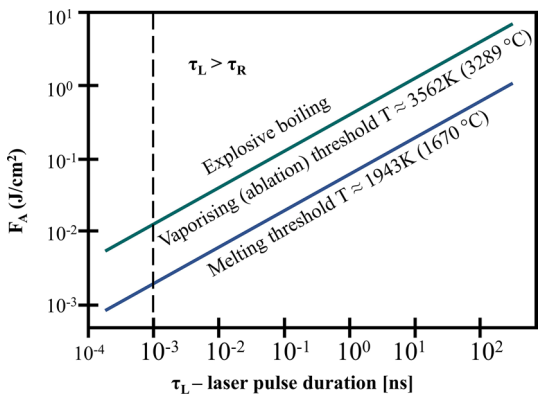

Fig. 8 Threshold fluence of melting and vaporizing for the Ti6Al4V titanium alloy at different pulse duration [20]

The laser beam is characterized by the Gaussian spatial fluence profile. The materials' surface starts melting and vaporizing in the peak on-axis Gaussian beam. In effect, the molten material fills the initially formed groove. As the pulse energies and temperature of the melted materials increase, the radial velocity of the melt increases too (Fig. 9) [43]. Once the kinetic energy of the liquid metal increases (above the vaporizing line in Fig. 8), the material starts to be ejected from the groove in the form of liquid droplets and jets (explosive boiling). Very intensive boiling, called the explosive mechanism, was reported at a critical temperature of 7225 K for the Ti6Al4V alloy according to the results obtained by Miottelo and Kelly [44] and Bulgakova [45]. The explosive mechanism corresponds to the micro-bulge structure and the formation of circular particles. Similar relationships were reported by Yibas et al. [46].

Based on the morphological analysis of the samples after the texturing process, additional tests were performed to characterize the samples' hardness, microstructure, and wear resistance. Samples of the P3 series were selected for these tests. Moreover, these samples exhibited a regular texture pattern and the greatest groove depths of the texture profile samples.

Based on the hardness measurements, P3 samples exhibited greater hardness values after the texturing process compared to samples in the initial state (P_is). The mean value of the Vickers hardness for the P3 samples group was 394 HV1, which was 15% greater than the mean value for samples in the initial state (349 ± 8 HV1). Microstructure morphology and grain size have an important influence on microhardness. The base Ti6Al4V alloy is a typical duplex alloy with Ti_α and Ti_β phases, which were reported for the initial state samples (Fig. 10a). Based on the EBSD analysis, grain refinement (Ti_α phase) for P3 samples was observed due to high solidification rates during the laser processes (Fig. 10b). However, the percentage share of the Ti_β phase in the structure was not estimated due to large areas of unidentified pixels. Therefore, P3 samples exhibited an optimal wear resistance compared to all of the samples due to the existence of finer α/α' grains. Similar results were presented by Grabowski et al. [42]. Ren et al. [47] indicated that the main reasons for the grain refinement of the tested Ti6Al4V titanium alloy in the laser texturing process are twinning deformation and dislocation movement. According to the Hall–Petch Eq. (4), it can be concluded that the grain refinement effect is positively correlated with the surface hardness of the material:

$$H_v = H_{v_0} + K_{Hv} d^{-1/2} \tag{4}$$

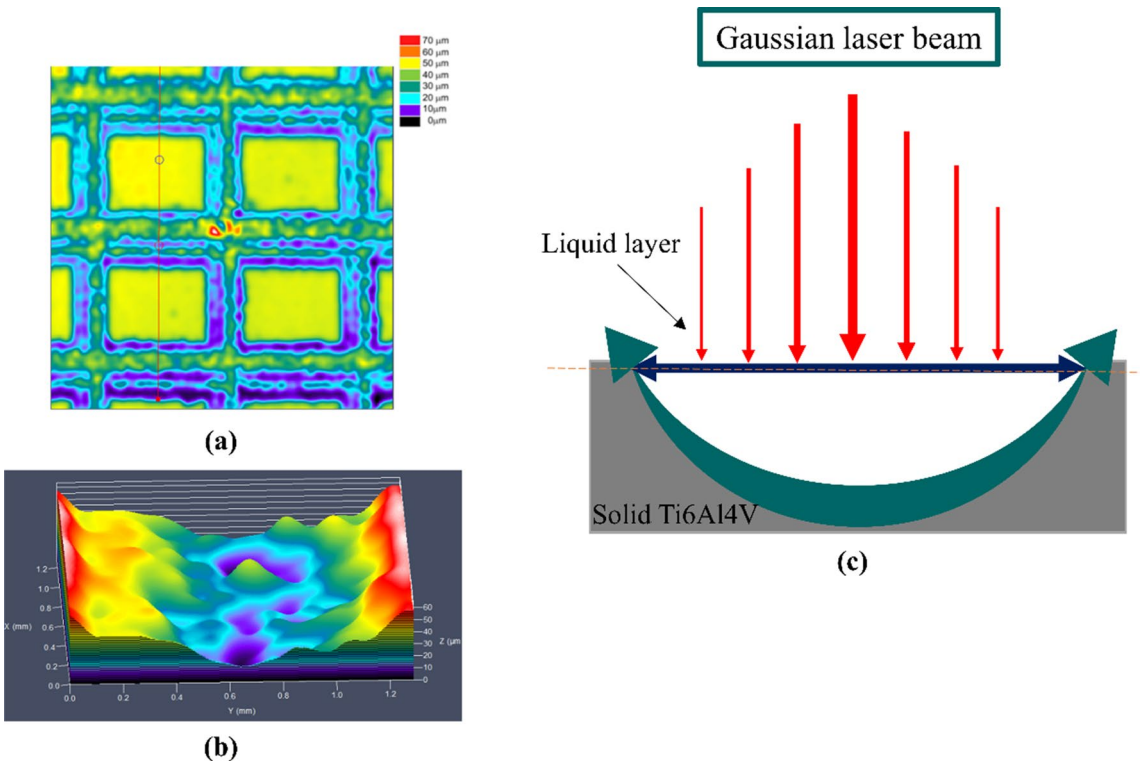

Fig. 9 Laser structured samples with a square pattern of grooves: **a** confocal microscopy images of the 2D topography and **b** 3D representation of a single path as well as **c** a schematic of the Gaussian laser beam

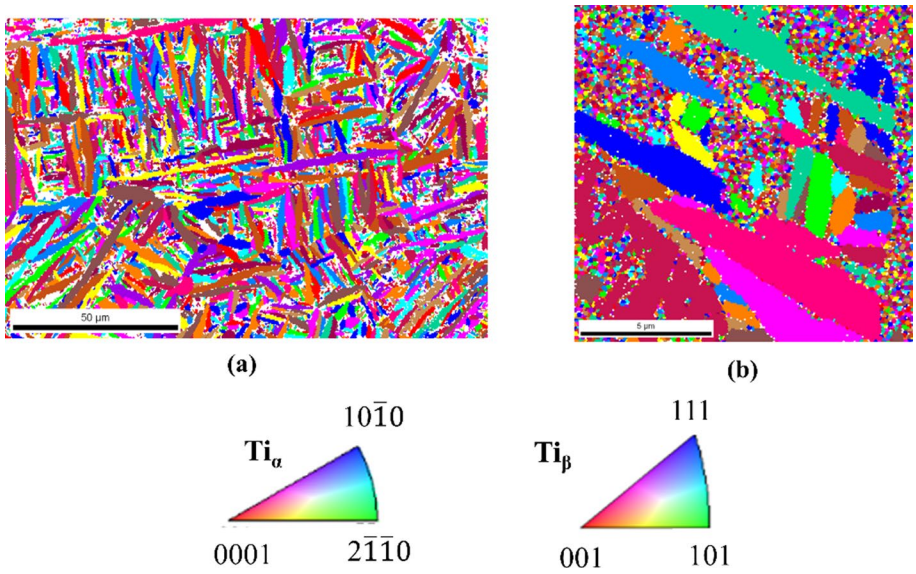

Fig. 10 EBSD microstructure analysis of: **a** initial and **b** P3 samples in the XY plane

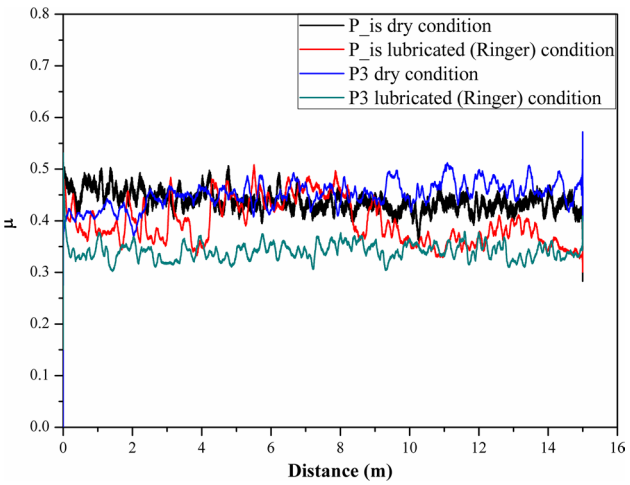

Fig. 11 Results of wear tests illustrated using the frictional coefficient profile for initial state samples and for P3 textured samples in different test conditions

where H_v—microhardness of the treated samples, H_{v0}—microhardness of untreatment samples, K_{H0}—constant, d—grain size (μm).

Figure 11 presents examples changes in the coefficient of friction with time during wear tests for initial state and P3 laser surface textured samples against a ceramic (Al_2O_3) ball at an applied load of 6 N.

The initial decrease in the coefficient of friction was observed for the initial state samples regardless of the test condition (Fig. 11). The point contact between the two surfaces (the tested samples and the Al_2O_3 ceramic ball) during the running-in stage results in the rapid increase in the local compressive pressure and shear stress. As a result, the surfaces of the frictional couple sequentially deform, fragment, and wear faster. As suggested by Fellah [48] and Ju [33], with increased sliding time, the contact area gradually increases with a decrease in the surface roughness of the tested sample and ceramic ball. In effect, the pressure was reduced, which progressively stabilized the friction coefficient. Additionally, the increased coefficient of friction at the first sliding time may be caused by damage and tearing of the oxide layer, which was formed on the substrate material. After this point, the ceramic ball completely touched the substrate of the tested sample. Also, the gas molecular film on the surface of the Al_2O_3 reduced the friction coefficient of the sample at the beginning of the test [49]. For initial state samples tested in dry conditions, the coefficient of friction maintained a steady state after the distance was greater than 4 m. However, for the samples tested in Ringer solution (Fig. 11), a decrease in the coefficient of friction was reported, due to the presence of wear debris between the surfaces. No visible stabilization of the coefficient of friction over the investigated range was recorded. For the P3 laser textured samples tested in dry conditions, an initial increase in the coefficient of friction with subsequent stabilization at distances greater than 2.5 m was observed (Fig. 11). For the samples tested in Ringer solution, the coefficient of friction plot was stable over the entire distance (up to 15 m) (Fig. 11). Additionally, the fluctuations in the friction coefficient were visible for all of the tested samples, regardless of testing conditions. There were fewer friction coefficient fluctuations for the treated surfaces compared to the initial state samples, indicating that a textured pattern surface has a more stable friction coefficient than the Ti6Al4V alloy surface. In general, the laminar titanium alloy materials formed by wear extrusion of debris adhere on the worn surface, leading to the fluctuation of friction coefficient, as indicated by [50]. Moreover, this

may be due to the increase in sample surface roughness following laser treatment, as revealed by Wu et al. [51].

Figure 12 presents variations in the coefficient of friction for both P3 and initial state samples, tested in dry and lubricated conditions.

The average values of the friction coefficients during the sliding process were calculated as average friction coefficients from the 5-times test for comparison. As shown in Fig. 12a, the value of the friction coefficient of the initial state sample surface tested in dry conditions was in the range of 0.44–0.45, regardless of the normal force used. The friction test confirmed that Ti6Al4V alloy was characterized by low wear resistance due to insufficient hardness (as presented in section Vickers hardness test) and an unstable friction coefficient. Similar results were reported by Yuan [49]. For the untreated samples tested under lubricated-sliding conditions, the coefficients of friction decreased to 0.39–0.41. For samples with a pattern of cross-like micro-grooves, the average coefficient of friction during the dry-conditions test was maintained at a similar level (0.41–0.42), regardless of the normal load used. The friction coefficient for the P3 samples slightly increased as the load increased above 3 N. Tang et al. [40] suggested that may be caused by both the micro-pattern deformation on the surface and a decrease in the performance of this structure to support an incremental increase of the load. Additionally, the deformation of the texture pattern increases the contact area between the surface and the ceramic ball. However, the surface deformation directly depended on the surface's hardness. By the assumptions of Ehtemam–Haghighi [52], surfaces characterized by increased hardness exhibit less initial plastic deformation, resulting in greater wear resistance. Due to the hardness of the P3 samples (more than 390 HV1), there is only a slight deformation under the 6 and 9 N loads, which has little effect on the performance of the texture pattern. Additionally, the slight deformation may increase the roughness of the surface, thereby leading to a decrease in friction coefficient. The coefficient of friction was reduced by 17% for laser-textured sample surfaces under lubricated-sliding wear test conditions compared to the value obtained during the dry-condition test. Furthermore, 26% reduction in friction coefficient was observed compared to the smooth, untextured surface samples under lubricated conditions. The average friction coefficients ranged from 0.34 to 0.35 for textured samples under lubricated conditions and were similar to the values reported by Conradi et al. [6] for pattern lines oriented perpendicularly or at 45° to the sliding direction, which suggested that the grooves and cavities are reservoirs of lubricant. Xu et al. [53] demonstrated that the friction coefficient was determined by the contact state, the actual contact area, and the lubrication of the interface.

Figure 13 provides the wear volume and wear rate coefficient as a function of normal load for both P_is initial state and P3 textured samples.

Under lubricated conditions, the wear volume and wear rate coefficients (Fig. 13a and b) of the non-textured samples are reduced compared to the results obtained under dry-sliding conditions. However, the recorded changes in both wear volume and wear rate coefficient for the tests under lubrication conditions were ~ 11% lower than those tested under dry conditions. Therefore, under the investigated conditions, Ringer's solution does not provide a lubrication film when combined with Ti6Al4V. Thus, the friction is

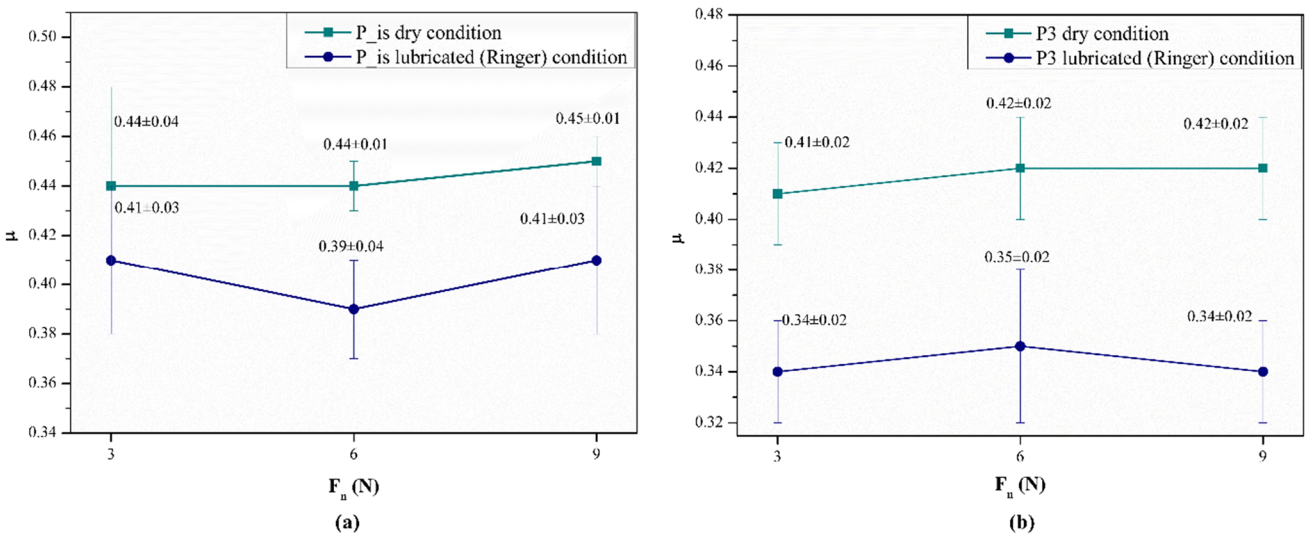

Fig. 12 The variations of the coefficient of friction as a function of various forces for: **a** initial state (P_is) and **b** P3 texturing process samples tested in different conditions (dry or lubricated)

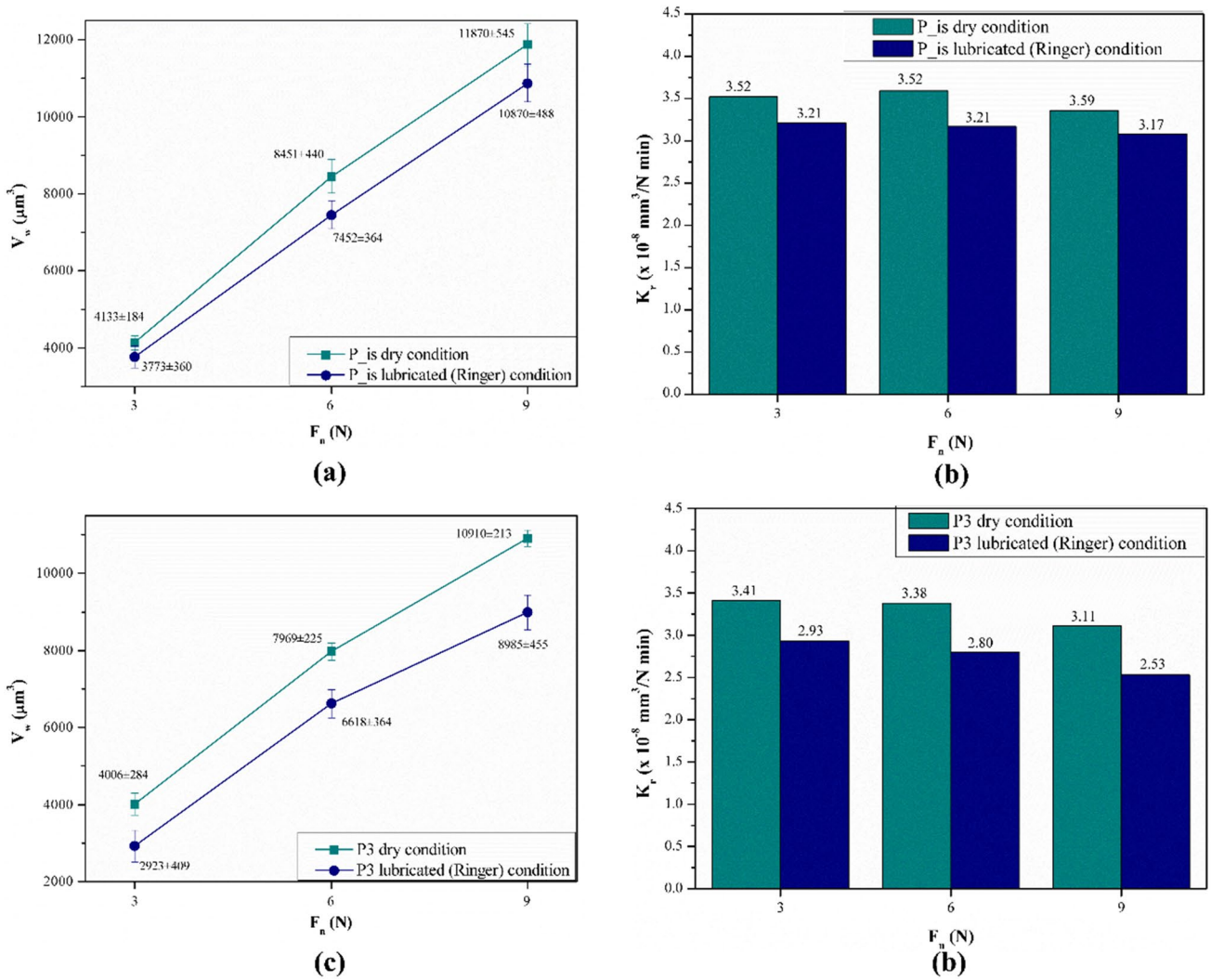

Fig. 13 The wear characteristic parameters: **a** wear volume and **b** wear rate coefficient for initial state (P_is) samples. The (**c**) wear volume and (**d**) wear rate coefficient for samples after the P3 texturing process P3

purely material dependent. Similar results of the wear test for Ti6Al4V alloy in Hank's solution were presented by Conradi et al. [6]. The reported values of the wear volume and calculated wear rate coefficient values for P3 textured samples tested under dry conditions were similar to those obtained for initial state samples tested in the same conditions. Under dry conditions, the average wear volumes for the P3 samples were ~ 4 ($F_n = 3$ N) to 8% ($F_n = 9$ N) less than the values obtained for the P_is, untextured samples. In the case of the crosshatched pattern samples, the wear rate and wear rate coefficient decreased for the lubricated contact. Moreover, a reduction in the volume of wear by up to 29% was noted. Additionally, for both P_is and P3 samples, as the normal load increased, the wear volume V_r increased proportionally, regardless of the test conditions. However, the wear rate coefficient decreased with increasing normal load, especially during tests under lubricated conditions. The coefficient of wear for the initial, untextured samples (Ringer solution conditions), slightly decreased at loads greater than 3 N. In contrast, the coefficient of wear for P3 samples decreased by more than 16 and 10% at 3 and 6 N loads, respectively, compared to 9 N loads.

P3 textured samples exhibited the lowest wear volume and wear rate coefficient, revealing that the wear resistance of P3 samples is greater than that of as-fabricated SLM samples. Additionally, the wear volume is compatible with the Archard's law (5) [54].

$$V = K\frac{F_n L}{H} \tag{5}$$

where V_w—wear volume (mm^3), L—tangential relative slip distance (mm), F_n—normal load (N), H—hardness of the material, K—constant wear factor

The wear volume of the material is inversely proportional to the hardness of the material. Therefore, the harder the material is, the better its wear resistance, which complements the previously presented assumptions of Ehtemam–Haghighias well as the microhardness measurements and microstructure analysis results (Fig. 9)—surfaces characterized by increased hardness exhibit less initial plastic deformation, resulting in greater wear resistance. Microstructure morphology and grain size have an important influence on microhardness. According to the presented in our work results of EBSD analysis, grain refinement (α-Ti phase) for P3 samples was observed due to high solidification rates during the laser processes. In general, in the untreated Ti6Al4V alloy, it could be seen that the main phase is α-Ti and the minor β-Ti phase was segregated at the grain boundaries. After the laser texturing process, the microstructure of the Ti6Al4V changes because the α-Ti phase was transformed into β-Ti, this transformation called β-transus, occurs at temperature 1268 K. In effect rapid solidification, the β-Ti phase is a matrix for fine recrystallized submicron grain phase α′-Ti (diffusionless transformations). A finer microstructure promotes better hardness and in effect wear behavior.

Additionally, according to the Coulomb's law, the coefficient friction (μ) can be calculated according to the Eq. 6:

$$\mu = \frac{F_f}{F_n} \tag{6}$$

where F_f—friction force (N), F_n—normal load (N).

In general, the coefficient friction changes with the friction force, generated during the wear process (after fixed normal load). Johanson et. al. [55] indicated that the adhesion force ($F_{f,adh}$) and surface furrowing effect ($F_{f,pl}$) have a significant effect on the friction force, as shown in Eq. 7:

$$F_f = F_{f,adh} + F_{f,pl} \tag{7}$$

where $F_{f,adh}$—adhesion force (N), $F_{f,pl}$—surface furrowing effect force (N).

The adhesion force can be determined by shear strength (τ) and the actual contact area (Ar), as shown in Eq. 8.

$$F_{f,adh} = \tau + A_t \tag{8}$$

where τ—shear strength (MPa), At—contact area (m^2).

Our research showed, that samples after the laser texturing process (P3) were characterized by the lower values of the coefficient friction and the wear volume compared to the nontreatment samples. It was found that the wear debris, generated during the wear process might be entrapped into the micro-groove structure (Fig. 14). That results in the reduction of wear debris on the surface. Laser texturing can also contribute to improved fatigue resistance by introducing compressive residual stresses in the textured regions. This can counteract the tensile stresses induced during cyclic loading, reducing the likelihood of fatigue cracks and wear-related failure. Additionally, at a low line density for textured samples, the concentration of hard wear particles generated by smoothing the bulges can be more effectively accommodated. In this case, fluid can be pushed along the lines, which are also quickly filled up with the bulge wear particles. Thus appropriate conditions for a lifting effect and good lubrication-film formation are prevented (Fig. 14). Bowsehera et al. [56]. Also, due higher microhardness of the samples with micro-grooves systems, the shedding of debris was reduced, owing to the reduction of residual stress at the interface of the titanium alloy and Al_2O_3 counter-samples (ball) during the friction process. In effect, the deformation friction force could be lowered. Furthermore, for the samples after the textured process, the actual contact area at the friction interface became smaller than for the samples in the initial state. This leads to the reduction of the adhesive friction force. During the wear test, under lubrication conditions, the micro-grooves system also can be a lubricant storage tank. Similarly, the adhered wear particles also reduce the stress concentration at the point of contact of the ball with the disc as suggested by Pfleging et al. [57], Qin et al. [58], and

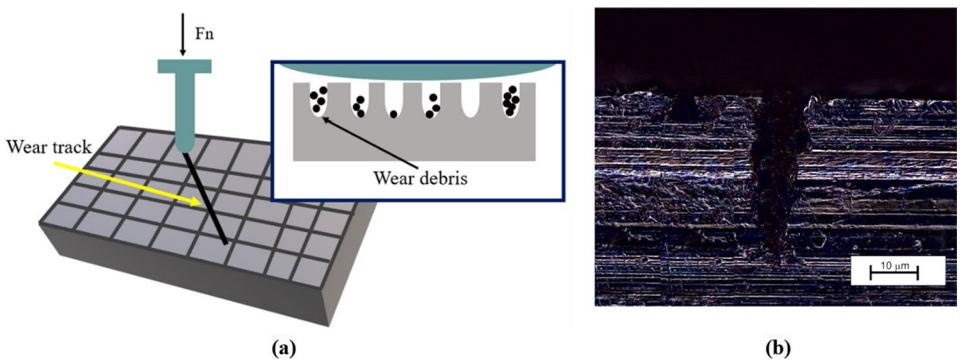

Fig. 14 **a** Scheme depicting the wear of textured samples and entrapped wear debris, **b** entrapped wear debris for P3 samples group after 15 min of sliding test

Varenberg et al. [59]. In effect, entrapped wear debris into grooves, they do not undergo active reactions with periprosthetic tissues, thus reducing the risk of failure caused by osteolysis. Additionally, the number of scratches on impact surfaces may be reduced. Wear damage for textured surfaces can be also associated with the ability to provide an extra hydrodynamic pressure which provides additional lifting force to the bearing surfaces and subsequently results in the separation of two articulating surfaces. In effect, the thickness of the lubrication film could increase.

The wear characteristics of all tested samples are investigated as they significantly affect the functional performance and durability of artificial joints. The morphologies of the wear tracks and worn surfaces ($F_n = 6$ N) were observed using SEM, as shown in Fig. 15. For all tested samples typical features of the abrasive wear mechanism were observed. In general, abrasive wear causes damage to the bearing surface of artificial joints in effect abrasion and formation of large quantities of bioactive wear debris. For the initial state samples tested in dry condition (Fig. 15a and b) numerous grooves and furrows aligned in the direction of sliding, and wear debris adhered to the surface were observed. The existence of the wear debris and its participation in the friction sliding process on the sample surface suggested the friction form may be transformed from two-body wear (tested samples and the Al_2O_3 counter ball sample) into three-body wear, which facilitates plastic deformation and wear damage, as suggested Kim et al. [60]. The wear debris formed by two-body wear together with natural bone can act as a cutting tool between two contact surfaces. Also, Bowsher and Shelton [56] based on results from the hip joint simulator, indicate that the hard particles have proven to cause deterioration to the bearing surfaces of implanted joints. In addition, for the samples in the initial state tested in dry conditions fatigue wear produces numerous fractures, vertical cracks, and spalling pits. Oxide particles were observed on the worn surface of the tested samples under high magnification. Ti6Al4V chemically reacts with oxygen in the environment to form oxides that are not capable of resisting damage during cyclic loading, thus resulting in oxidative wear. A similar trend was observed for the samples tested in Ringer solution (lubricated conditions) (Fig. 15c and d). For the P3 laser textured samples, the wear surfaces were smoother, and the presence of the smooth surface could be observed, which indicated relatively milder wear regardless of the test conditions (Fig. 15c and d). Additionally, it was found that almost all the textured surfaces have a uniform wear pattern. Fewer micro-cracks were observed for the samples after the texturing process (both conditions) compared to the samples in the initial state. The texture patterns were not completely removed as a result of the wear test. It was found, that the wear debris particles may be entrapped inside the dimples, which leads to a reduction in the coefficient of friction due to the cushioning effect.

The presence of oxides on the worn surface of textured samples (especially under dry condition tests) could be attributed to surface oxidation during texturing and its presence in the original microstructure. The hardness values

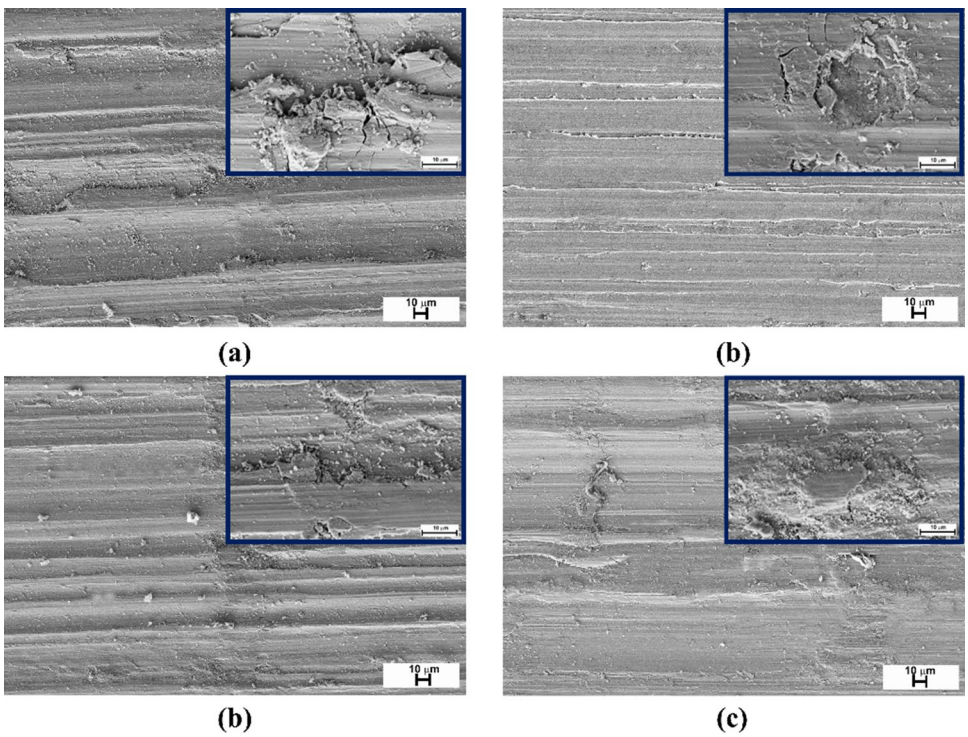

Fig. 15 SEM micrographs revealing the surface morphologies of the wear track for initial state samples post-wear test under **a** dry and **b** lubricated conditions as well as P3 textured samples post-wear tests under **c** dry and **d** lubricated conditions

of Al_2O_3, TiO, and TiO_2, the most frequently identified oxides, are equal to 19.60, 19.40, and 4.60 GPa, respectively [33]. Oxides formed during friction processes may loosen, which, combined with their brittleness, may result in loss of cohesion with the base material and may act as wear debris. That is why important is the possibility of entrapped wear debris (also oxides) into groove.

The wear debris is presented in Fig. 16. Based on the obtained results, it can be observed that for both sample groups tested under the Ringer solution, wear debris with different surface features can be identified. This suggests that they exhibit different wear mechanisms, specifically adhesive wear and oxidative wear marked by 1, while delamination wear is marked by 2. Debris marked by 1 appears in the form of a granulated structure, and EDS analysis reveals titanium and oxygen as the main compositions, indicating that the debris is derived from titanium oxide. In contrast, debris marked by 2 is in the form of metallic flakes, and EDS analysis suggests that it originates from the delamination of the titanium alloy. For the untreated samples, the predominant wear debris is large, plate-like, and irregular in shape. However, the wear debris from laser-textured samples (P3), tested under the same conditions, exhibit a small, irregular, and blocky shape of transferred fragments.

In summary, the micro-texturing process stands out as one of the methods for enhancing surface lubrication and tribological performance on functional surfaces for biomedical applications. However, the optimized laser texturing pattern and its geometrical parameters are still under investigation. The focus is particularly interesting for improving the tribological behavior of metal biomaterials such as Ti6Al4V ELI through laser texturing. Conradi et al. [6] applied laser-texturing to manipulate the Ti6Al4V's surface by preparing three different laser-textured patterns with varying densities: lines, crosshatching (texture densities: 40, 45–20, and 25%, line separation $\Delta x = 100$, 180, and 280 µm, $\Delta y = 280$ µm), and dimples (texture density: 50%). The coefficient of friction improvement was observed

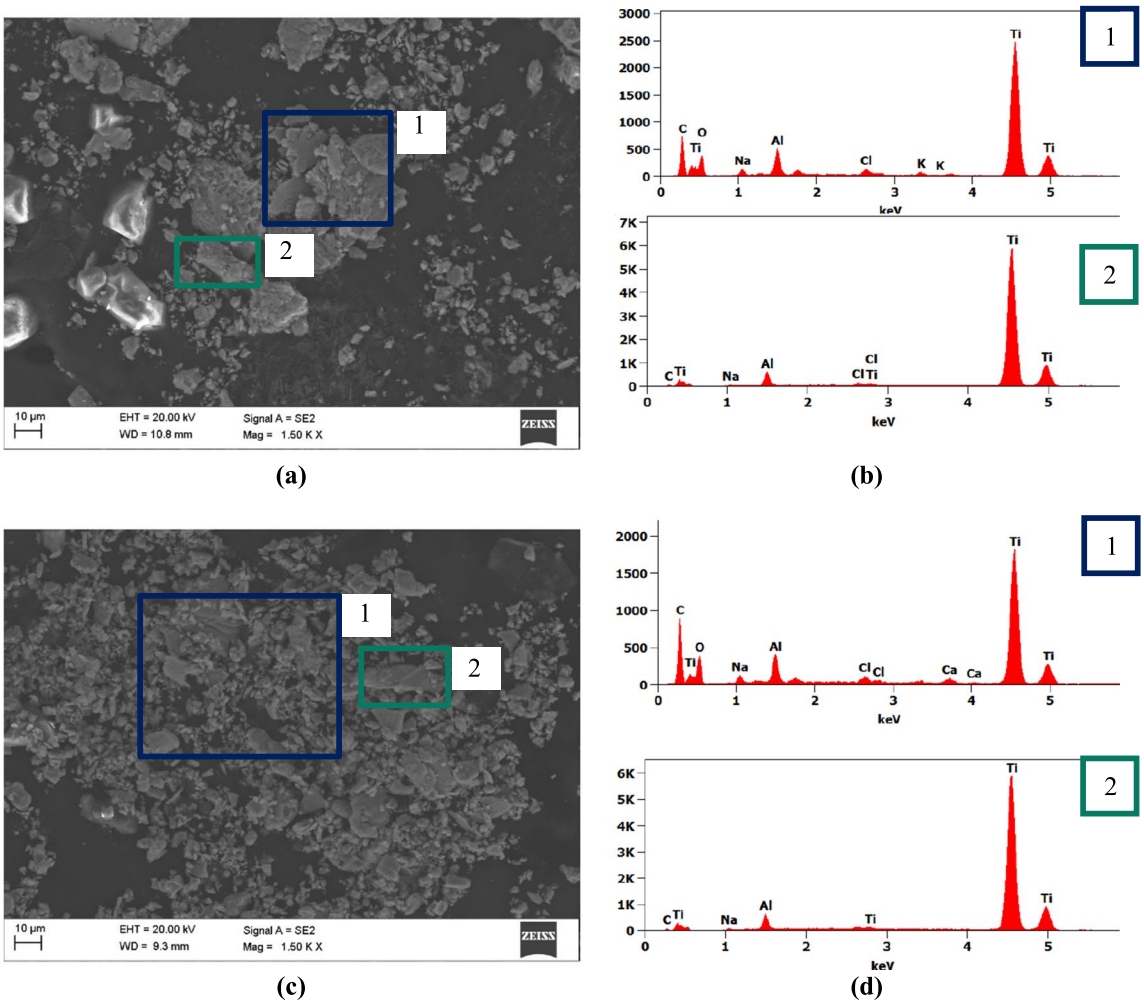

Fig. 16 SEM images and EDS spectra of wear debris (**a**) and (**b**) P_is, (**c**) and **d** P3

for laser-textured surfaces. For line-and crosshatching texture, the better wear behavior was most pronounced for the small texturing density, resulting in a decrease of the coefficient of friction from 0.5 for untreated Ti6Al4V to 0.35 under Hank's solution conditions, this coincides with our findings. In addition, the provided information indicates a significant effect of the texture pattern density ratio on wear behavior. In our work, the laser texture pattern was characterized by a 17% density ratio. Also, Cao et al. [61] demonstrated that textured samples with a dimple density of 25% exhibited the lowest wear rate compared to samples with dimple densities of 35 and 60%. However, Conradi et al. [6] also showed, interesting results were obtained for the dimples-textured surface, where the wear behavior improved both in dry and lubricated conditions. For future biomedical applications, it is crucial to consider that the surface topography must promote cell proliferation. In the majority of cases, cells tend to align and spread along topographical discontinuities such as the edges of grooves and ridges. Results showed by Kumari et al. [62] confirm the thesis. The study focuses on understanding the wear and bioactivity behaviors of laser-textured Ti6Al4V ELI with line and dimple geometry. It was found that laser texturing led to a decrease in wear rate, with the lowest magnitude of wear achieved for dimple texturing. However, cell adherence is lower for the dimple texture pattern compared to the line texture. On the surface with linear texturing, cells were preferentially attached along the direction of texturing in the textured zone. That is why dimples-texturing may not provide the best biocompatibility, despite good wear behaviour. In addition, the provided information indicates a significant effect of the texture pattern Interesting results were shown in the work of Velayuthaperumal et al. [23], as they investigated the influence of laser texture patterns in the form of dimples, moats, and a hybrid on the wettability and tribological characteristics of titanium alloy for medical applications. It was found that moat and hybrid-type textures exhibited better tribological properties. The wear depth was reduced by 82 and 75%, respectively, for moat and hybrid textures compared to untreated Ti6AL4V. The presented results encourage planning experiments for hybrid laser textures-crosshatching grooves and dimples.

Wang et al. [21] effectively reduced the coefficient of friction in dry sliding and improved the wear resistance of Ti6Al4V ELI titanium alloy through the laser texturing process. Researchers compared the wear behavior of textured samples with different groove widths, ranging from 25 to 65 µm. The results demonstrated that Ti6Al4V with a microgroove width of 45 µm exhibited excellent wear resistance, with decreasing wear rates of 90 and 85% under dry friction and SBF lubrication, respectively, compared to the Ti64 sample. Similarly, for samples with a groove width of 35 µm, researchers indicated good wear resistance with a decreasing wear rate of 78 and 81% under dry friction and SBF lubrication. Tiainen et al. [63] investigated the structural integrity of laser-textured Ti6Al4V alloy with cross-hatched micropatterns through friction tests against bone. It was found that the textured surfaces with a 40 µm groove width were characterized by having low-wear debris. Our results showed improved wear behavior, which was attributed to a decreased wear volume of 29% for the crosshatching texture with a groove width of 30 µm. However, we recommend further investigation into wider groove widths to ensure even better wear behavior, which might be associated with the increase in surface microhardness. Additionally, the heightened hardness was linked to the refinement of the titanium alloy's grain structure, impeding dislocation movement, a phenomenon also observed in our work. Many researchers in their works indicate [6, 21, 64], that the grains of textured samples are more refined than those of the untreated Ti6Al4V. In the microstructure, the α-Ti phase is dominant and contain a small amount of Ti-β. In addition, that closer the texture region is, the finer deposition at the bottom of the texture. Zhou et al. [65] demonstrated an increase in hardness after the LP process of 20 and 25%, compared to the Ti6Al4V alloy in its initial state. We observed a hardness increase of 17% after the laser texturing process.

4 Conclusion

Conducted research regarding the tribological behavior of the laser textured Ti6Al4V ELI allowed us to conclude that:

- The existence of the wear debris, and its participation in the friction sliding process on the sample surface, suggested the friction form may be transformed from the two-body wear (tested samples and the Al_2O_3 counter ball sample) into three-body wear, which leads to plastic deformation and wear damage.
- Ringer's solution does not provide a lubrication film when combined with Ti6Al4V and thus the friction is purely material-dependent.
- The surface texture imparted better wear behavior to the Ti6Al4V alloy under lubricated test conditions. The worn debris particles adhered to the surface may be entrapped inside the texture path, which leads to a reduced coefficient of friction due to the cushioning effect and reduces the stress concentration at the point of contact of the ball with the disc.

Authors' contributions All authors contributed to the study conception and design. Material preparation, data collection and analysis were

performed by Anna Woźniak, Janusz Szewczenko, Marcin Adamiak, Branislav Hadzima and Oktawian Bialas, first draft of the manuscript was written by Anna Woźniak, and Oktawian Bialas and all authors commented on previous versions of the manuscript. All authors read and approved the final manuscript.

Funding Publication supported under the Excellence Initiativ-Research University program at the Silesian University of Technology (pro-quality grant for high-scoring publications No. 10/100/RGJ22/0028).

Availability of data and materials The data that support the findings of this study are available from the corresponding author, [Anna Woźniak], upon reasonable request.

Code availability All data generated or analysed during this study are included in this published article.

Declarations

Conflict of interest The authors declare that they have no conflict of interest.

Ethics approval Not applicable.

References

1. Pereira CM, Pinto FFE, Nakagawa SA, Chung WT. Reconstruction with unconventional endoprostheses after resection of primary distal femoral bone tumors: implant survival and functional outcomes. Rev Bras Ortop. 2022;57:1030–8. https://doi.org/10.1055/S-0042-1748966.
2. Luqman M, Seikh AH, Sarkar A, Ragab SA, Mohammed JA, Ijaz MF, Abdo HS. A comparative study of the electrochemical behavior of α and β Phase Ti6Al4V alloy in ringer's solution. Crystals. 2020;10:190. https://doi.org/10.3390/cryst10030190.
3. Iwabuchi A, Lee JW, Uchidate M. Synergistic effect of fretting wear and sliding wear of Co-alloy and Ti-alloy in Hanks' solution. Wear. 2007;263:492–500. https://doi.org/10.1016/J.WEAR.2007.01.102.
4. Beake BD, Liskiewicz TW. Comparison of nano fretting and nano-scratch tests on biomedical materials. In: Beake BD, Liskiewicz TW, editors. of the tribology international. Amsterdam: Elsevier; 2013. p. 123–31.
5. Babis GC, Stavropoulos NA, Sasalos G, Ochsenkuehn-Petropoulou M, Megas P. Metallosis and elevated serum levels of tantalum following failed revision hip arthroplasty—a case report. Acta Orthop. 2014;85:677–80. https://doi.org/10.3109/17453674.2014.950816.
6. Conradi M, Kocijan A, Klobčar D, Podgornik B. Tribological response of laser-textured Ti6Al4V alloy under dry conditions and lubricated with Hank's solution. Tribol Int. 2021;160: 107049. https://doi.org/10.1016/J.TRIBOINT.2021.107049.
7. Reddy AR, Ismail S. Impact of multi-scaled surface textures on tribological performance of parallel sliding contact under lubricated condition. Tribol Int. 2023;183: 108415. https://doi.org/10.1016/J.TRIBOINT.2023.108415.
8. Tewelde FB, Zhou T, Zhou J, Guo W, Zhao B, Ge X, Wang W, Wang X, Wang X. Asymmetric surface texturing for directional friction control under dry sliding condition. Tribol Int. 2023;181: 108321. https://doi.org/10.1016/J.TRIBOINT.2023.108321.
9. Song S, Xiao G, Liu Y, Zhou K, Liu S, Huang J. Tribological response of groove-textured surface with compressive stress on Ti6Al4V processed by laser and abrasive belt. Tribol Int. 2023;180: 108265. https://doi.org/10.1016/J.TRIBOINT.2023.108265.
10. Wang C, Hong J, Cui M, Huang H, Zhang L, Yan J. The effects of simultaneous laser nitriding and texturing on surface hardness and tribological properties of Ti6Al4V. Surf Coatings Technol. 2022;437: 128358. https://doi.org/10.1016/J.SURFCOAT.2022.128358.
11. Huang J, Guan Y, Ramakrishna S. Tribological behavior of femtosecond laser-textured leaded brass. Tribol Int. 2021;162: 107115. https://doi.org/10.1016/J.TRIBOINT.2021.107115.
12. Lin N, Li D, Zou J, Xie R, Wang Z, Tang B. Surface texture-based surface treatments on Ti6Al4V titanium alloys for tribological and biological applications: a mini review. Materials. 2018;11:487. https://doi.org/10.3390/MA11040487.
13. Sadeghi M, Kharaziha M, Salimijazi HR, Tabesh E. Role of micro-dimple array geometry on the biological and tribological performance of Ti6Al4V for biomedical applications. Surf Coatings Technol. 2019;362:282–92. https://doi.org/10.1016/J.SURFCOAT.2019.01.113.
14. Pratap T, Patra K. Tribological performances of symmetrically micro-textured Ti-6Al-4V alloy for hip joint. Int J Mech Sci. 2020;182: 105736. https://doi.org/10.1016/J.IJMECSCI.2020.105736.
15. Yu Z, Yin S, Zhang W, Jiang X, Hu J. Picosecond laser texturing on titanium alloy for biomedical implants in cell proliferation and vascularization. J Biomed Mater Res Part B Appl Biomater. 2020;108:1494–504. https://doi.org/10.1002/JBM.B.34497.
16. Fiorucci MP, López AJ, Ramil A. Multi-scale characterization of topographic modifications on metallic biomaterials induced by nanosecond Nd:YVO4 laser structuring. Precis Eng. 2018;53:163–8. https://doi.org/10.1016/j.precisioneng.2018.03.009.
17. Yu Z, Yang G, Zhang W, Hu J. Investigating the effect of picosecond laser texturing on microstructure and biofunctionalization of titanium alloy. J Mater Process Technol. 2018;255:129–36. https://doi.org/10.1016/j.jmatprotec.2017.12.009.
18. Kashyap V, Ramkumar P. Feasibility study of micro-groove cross hatched surface texturing on Ti6Al4V for improved biotribological performance in metal-on-polymer hip implant. Tribol Mater Surfaces Interfaces. 2019;13:150–60. https://doi.org/10.1080/17515831.2019.1606582.
19. Wang Y, Ke C, Wu T, Zhao X, Wang R. Nanosecond laser texturing with hexagonal honeycomb micro-structure on titanium for improved wettability and optical properties. Optik (Stuttg). 2019;192: 162953. https://doi.org/10.1016/j.ijleo.2019.162953.
20. Grabowski A, Sozańska M, Adamiak M, Kępińska M, Florian T. Laser surface texturing of Ti6Al4V alloy, stainless steel and aluminium silicon alloy. Appl Surf Sci. 2018;461:117–23. https://doi.org/10.1016/j.apsusc.2018.06.060.
21. Wang C, Tian P, Cao H, Sun B, Yan J, Xue Y, Lin H, Ren T, Han S, Zhao X. Enhanced biotribological and anticorrosion properties and bioactivity of Ti6Al4V alloys with laser texturing. ACS Omega. 2022;7:31081–97.

22. Li LX, Li ZX, Xing ZG, Guo WL, Huang YF, Wang HD. Effect of femtosecond laser bionic texture on anti-wear properties of medical Ti-6Al-4 V. Tribol Int. 2023;190: 109062. https://doi.org/10.1016/J.TRIBOINT.2023.109062.
23. Velayuthaperumal S, Radhakrishnan R. Effect of different laser texture configurations on improving surface wettability and wear characteristics of Ti6Al4V implant material. J Brazilian Soc Mech Sci Eng. 2023;45:1–14. https://doi.org/10.1007/S40430-023-04287-7/FIGURES/10.
24. PN-EN ISO 5832-3:2017-02 Metallic materials—part 3: titanium alloy 6-aluminium 4-vadandium. Geneva, Switzerland, 2017.
25. Woźniak A, Adamiak M. The influence of the slm process parameters optimization on the density and microstructure of Ti6Al4V alloy. Int J Mod Manuf Technol. 2020;12:129–36.
26. Mahmud G, Campbell CJ, Bishop KJM, Komarova YA, Chaga O, Soh S, Huda S, Kandere-Grzybowska K, Grzybowski BA. Directing cell motions on micropatterned ratchets. Nat Phys. 2009;5(8):606–12. https://doi.org/10.1038/nphys1306.
27. Raimbault O, Benayoun S, Anselme K, Mauclair C, Bourgade T, Kietzig AM, Girard-Lauriault PL, Valette S, Donnet C. The effects of femtosecond laser-textured Ti-6Al-4V on wettability and cell response. Mater Sci Eng C. 2016;69:311–20. https://doi.org/10.1016/J.MSEC.2016.06.072.
28. Chebolu A, Laha B, Ghosh M. Nagahanumaiah investigation on bacterial adhesion and colonisation resistance over laser-machined micro patterned surfaces. Micro Nano Lett. 2013;8:280–3. https://doi.org/10.1049/mnl.2013.0109.
29. Veiko V, Karlagina Y, Zernitckaia E, Egorova E, Radaev M, Yaremenko A, Chernenko G, Romanov V, Shchedrina N, Ivanova E, et al. Laser-induced μ-rooms for osteocytes on implant surface: an in vivo study. Nanomater. 2022;12:4229. https://doi.org/10.3390/NANO12234229.
30. Fisher J, Dowson D, Hamdzah H, Lee HL. The effect of sliding velocity on the friction and wear of UHMWPE for use in total artificial joints. Wear. 1994;175:219–25. https://doi.org/10.1016/0043-1648(94)90185-6.
31. Houdková Š, Šperka P, Repka M, Martan J, Moskal D. Shifted laser surface texturing for bearings applications. J Phys Conf Ser. 2017;843:012076. https://doi.org/10.1088/1742-6596/843/1/012076.
32. Wang C, Zhang G, Li Z, Zeng X, Xu Y, Zhao S, Hu H, Zhang Y, Ren T. Tribological behavior of Ti-6Al-4V against cortical bone in different biolubricants. J Mech Behav Biomed Mater. 2019;90:460–71. https://doi.org/10.1016/J.JMBBM.2018.10.031.
33. Ju J, Zhou Y, Wang K, Liu Y, Li J, Kang M, Wang J. Tribological investigation of additive manufacturing medical Ti6Al4V alloys against Al_2O_3 ceramic balls in artificial saliva. J Mech Behav Biomed Mater. 2020;104: 103602. https://doi.org/10.1016/j.jmbbm.2019.103602.
34. Huerta-Murillo D, García-Girón A, Romano JM, Cardoso JT, Cordovilla F, Walker M, Dimov SS, Ocaña JL. Wettability modification of laser-fabricated hierarchical surface structures in Ti-6Al-4V titanium alloy. Appl Surf Sci. 2019;463:838–46. https://doi.org/10.1016/j.apsusc.2018.09.012.
35. Wang Q, Wang H, Zhu Z, Xiang N, Wang Z, Sun G. Switchable wettability control of titanium via facile nanosecond laser-based surface texturing. Surf Interfac. 2021;24: 101122. https://doi.org/10.1016/j.surfin.2021.101122.
36 Hamad AH. Effects of different laser pulse regimes (nanosecond, picosecond and femtosecond) on the ablation of materials for production of nanoparticles in liquid solution. In: Hamad AH, editor. High energy and short pulse lasers. London: InTech; 2016.
37. Mannion PT, Magee J, Coyne E, O'Connor GM, Glynn TJ. The effect of damage accumulation behaviour on ablation thresholds and damage morphology in ultrafast laser micro-machining of common metals in air. Appl Surf Sci. 2004;233:275–87. https://doi.org/10.1016/j.apsusc.2004.03.229.
38. Giorleo L, Montesano L, La Vecchia GM. Laser surface texturing to realize micro-grids on DLC coating: effect of marking speed, power, and loop cycle. Int J Precis Eng Manuf. 2021;22:745–58. https://doi.org/10.1007/s12541-021-00498-x.
39. Hauert R. An overview on the tribological behavior of diamond-like carbon in technical and medical applications. Tribol Int. 2004;37:991–1003. https://doi.org/10.1016/J.TRIBOINT.2004.07.017.
40. Tang MK, Huang XJ, Yu JG, Li XW, Zhang QX. The effect of textured surfaces with different roughness structures on the tribological properties of al alloy. J Mater Eng Perform. 2016;25:4115–25. https://doi.org/10.1007/s11665-016-2251-9.
41. Palik E. Handbook of Optical Constans of solid. In: Palik ED, editor. 3 Academic Press. Cambridge; 1991. (**978-0-12-544422-4**).
42. Grabowski A, Florian T, Wieczorek J, Adamiak M. Structuring of the Ti6Al4V alloy surface by pulsed laser remelting. Appl Surf Sci. 2021;535: 147618. https://doi.org/10.1016/j.apsusc.2020.147618.
43 Bulgakova NM, Bulgakov AV. Pulsed laser ablation of solids: transition from normal vaporization to phase explosion. Appl Phys A. 2001;73:199–208. https://doi.org/10.1007/S003390000686.
44 Miotello A, Kelly R. Laser-induced phase explosion: new physical problems when a condensed phase approaches the thermodynamic critical temperature. Appl Phys A. 1999;69:S67–73. https://doi.org/10.1007/S003399900296.
45 Bulgakova NM, Bulgakov AV, Bourakov IM, Bulgakova NA. Pulsed laser ablation of solids and critical phenomena. In: Bulgakova NM, Bulgakov AV, Bourakov IM, Bulgakova NA, editors. of the Applied Surface Science. Amsterdam: Elsevier; 2002. p. 96–9.
46. Yilbas BS, Ali H, Al-Sharafi A, Al-Qahtani H. Laser processing of Ti6Al4V alloy: wetting state of surface and environmental dust effects. Heliyon. 2019;5: e01211. https://doi.org/10.1016/j.heliyon.2019.e01211.
47. Wu SQ, Lu YJ, Gan YL, Huang TT, Zhao CQ, Lin JJ, Guo S, Lin JX. Microstructural evolution and microhardness of a selective-laser-melted Ti-6Al-4V alloy after post heat treatments. J Alloys Compd. 2016;672:643–52. https://doi.org/10.1016/j.jallcom.2016.02.183.
48. Fellah M, Labaïz M, Assala O, Dekhil L, Taleb A, Rezag H, Iost A. Tribological behavior of Ti-6Al-4V and Ti-6Al-7Nb Alloys for total hip prosthesis. Adv Tribol. 2014. https://doi.org/10.1155/2014/451387.
49. Yuan S, Lin N, Zou J, Lin X, Liu Z, Yu Y, Wang Z, Zeng Q, Chen W, Tian L, et al. In-situ fabrication of gradient titanium oxide ceramic coating on laser surface textured Ti6Al4V alloy with improved mechanical property and wear performance. Vacuum. 2020;176: 109327. https://doi.org/10.1016/J.VACUUM.2020.109327.
50. Wang K, Xiong D, Niu Y. Novel lubricated surface of titanium alloy based on porous structure and hydrophilic polymer brushes. Appl Surf Sci. 2014;317:875–83. https://doi.org/10.1016/J.APSUSC.2014.09.014.
51. Wu Z, Xing Y, Huang P, Liu L. Tribological properties of dimple-textured titanium alloys under dry sliding contact. Surf Coatings Technol. 2017;309:21–8. https://doi.org/10.1016/J.SURFCOAT.2016.11.045.
52. Ehtemam-Haghighi S, Prashanth KG, Attar H, Chaubey AK, Cao GH, Zhang LC. Evaluation of mechanical and wear properties of TixNb7Fe alloys designed for biomedical applications. Mater Des. 2016;111:592–9. https://doi.org/10.1016/J.MATDES.2016.09.029.
53. Xu J, Hu W, Xie ZH, Munroe P. Reactive-sputter-deposited β-Ta2O5 and TaON nanoceramic coatings on Ti-6Al-4V alloy

against wear and corrosion damage. Surf Coatings Technol. 2016;296:171–84. https://doi.org/10.1016/J.SURFCOAT.2016.04.004.
54. Archard JF. Contact and rubbing of flat surfaces. J Appl Phys. 1953;24:981–8. https://doi.org/10.1063/1.1721448.
55. Johnson KL, Greenwood JA. An adhesion map for the contact of elastic spheres. J Colloid Interface Sci. 1997;192:326–33. https://doi.org/10.1006/JCIS.1997.4984.
56. Bowsher JG, Shelton JC. A hip simulator study of the influence of patient activity level on the wear of crosslinked polyethylene under smooth and roughened femoral conditions. Wear. 2001;250:167–79. https://doi.org/10.1016/S0043-1648(01)00619-6.
57. Pfleging W, Kumari R, Besser H, Scharnweber T, Majumdar JD. Laser surface textured titanium alloy (Ti-6Al-4V): part 1—surface characterization. Appl Surf Sci. 2015;355:104–11. https://doi.org/10.1016/j.apsusc.2015.06.175.
58. Qin Y, Xiong D, Li J. Characterization and friction behavior of LST/PEO duplex-treated Ti6Al4V alloy with burnished MoS2 film. Appl Surf Sci. 2015;347:475–84. https://doi.org/10.1016/J.APSUSC.2015.04.134.
59. Varenberg M, Halperin G, Etsion I. Different aspects of the role of wear debris in fretting wear. Wear. 2002;252:902–10. https://doi.org/10.1016/S0043-1648(02)00044-3.
60. Kim SH, Jeong SH, Kim TH, Choi JH, Cho SH, Kim BS, Lee SW. Effects of solid lubricant and laser surface texturing on tribological behaviors of atmospheric plasma sprayed Al_2O_3-ZrO_2 composite coatings. Ceram Int. 2017;43:9200–6. https://doi.org/10.1016/J.CERAMINT.2017.04.073.
61. Cao L, Chen Y, Cui J, Li W, Lin Z, Zhang P. Corrosion wear performance of pure titanium laser texturing surface by nitrogen ion implantation. Met. 2020;10:990. https://doi.org/10.3390/MET10080990.
62. Kumari R, Scharnweber T, Pfleging W, Besser H, Majumdar JD. Laser surface textured titanium alloy (Ti-6Al-4V)—Part II—Studies on bio-compatibility. Appl Surf Sci. 2015;357:750–8. https://doi.org/10.1016/j.apsusc.2015.08.255.
63. Tiainen L, Abreu P, Buciumeanu M, Silva F, Gasik M, Serna Guerrero R, Carvalho O. Novel laser surface texturing for improved primary stability of titanium implants. J Mech Behav Biomed Mater. 2019;98:26–39. https://doi.org/10.1016/j.jmbbm.2019.04.052.
64. Xu Y, Li Z, Zhang G, Wang G, Zeng Z, Wang C, Wang C, Zhao S, Zhang Y, Ren T. Electrochemical corrosion and anisotropic tribological properties of bioinspired hierarchical morphologies on Ti-6Al-4V fabricated by laser texturing. Tribol Int. 2019;134:352–64. https://doi.org/10.1016/J.TRIBOINT.2019.01.040.
65. Zhou J, Sun Y, Huang S, Sheng J, Li J, Agyenim-Boateng E. Effect of laser peening on friction and wear behavior of medical Ti6Al4V alloy. Opt Laser Technol. 2019;109:263–9. https://doi.org/10.1016/J.OPTLASTEC.2018.08.005.